ELSEVIER

Journal of Power Sources 96 (2001) 57–67

JOURNAL OF POWER SOURCES

www.elsevier.com/locate/jpowsour

Analysis of power limitations at porous supercapacitor electrodes under cyclic voltammetry modulation and dc charge

Wendy G. Pell, Brian E. Conway*

Chemistry Department, University of Ottawa, 10 Marie Curie Street, Ottawa, Ont., Canada KIN 6N5

Received 28 November 2000; accepted 8 December 2000

Abstract

A simple capacitor is perceived as being capable of discharge (or recharge) at high rates, limited only by a small equivalent series resistance. However, in the case of electrochemical capacitors, based on high specific area porous electrode materials, power limitations arise due to the complex-distribution of electrolyte internal resistance, coupled with double-layer or pseudo-capacitative elements. The present paper quantitatively examines both numerically and experimentally the effects of internal electrolyte resistance as evaluated by the current-response functions for porous capacitor electrodes, generated in cyclic voltammetry (CV) experiments and for voltage versus time responses in dc charge/discharge regimes. © 2001 Elsevier Science B.V. All rights reserved.

Keywords: Electrochemical capacitors; Internal resistance; Cyclic voltammetry; Charge/discharge curves

1. Introduction

Electrochemical capacitors are based on utilisation of the distributed interface of conducting materials having large specific areas such as carbon felts, cloths, powders and aerogels [1], and also conducting metal oxides (RuO_2) [2], nitrides [3], or conducting polymers, including chemically or electrochemically generated RuO_2 deposits on carbon substrates [4,5].

At carbon surfaces, the capacitance arises mainly from electrostatic double-layer charging [6] while, for example, at RuO_2, it arises mainly from redox pseudo-capacitance (2,7] coupled with a smaller double-layer capacitance.

It is important to emphasise that electrochemical capacitors cannot functionally substitute for batteries; rather their applications and performance behaviour are *complementary* to those of rechargeable batteries. Elsewhere [8], we have delineated, in some detail, the similarities and differences between batteries and electrochemical capacitors for electrical energy storage and delivery. Primarily, electrochemical capacitors, now often referred to as ''supercapacitors'' [7], provide high-power performance but at low energy–densities and also with the advantage of large multiple cycle-life of ca. 100,000 cycles to deep depths of discharge, DOD. On the other hand, batteries provide high specific energy–densities but at relatively low operational power–densities and with limited recyclabilities, especially at appreciable DODs. This complementarity of performance has led to various proposed hybrid applications employing tandem configurations of battery and capacitor modules enabling optimisation of both power and energy–density performance [9].

The relationship between operational power–density (P) and simultaneously achievable energy–density (E) is commonly represented by so-called Ragone plots [10,11]. E tends to decrease as P drain is increased. In a capacitor, this effect is mainly due to internal ohmic (IR) drop which increases with current (I) drain into a load, lowering the voltage. In a battery, it is due to kinetic polarisation effects in addition to IR drop, together with significant effects arising from concentration gradients developed on charge or discharge. In operation of a capacitor device, for fundamental reasons, the Ragone relations are importantly dependent on state-of-charge [11] (SOC) since the operational voltage (V), is directly proportional to charge (Q), $V = Q/C$, so that both P and E are determined by SOC. In battery performance, related effects can arise but are secondary and smaller.

In electrochemical capacitors employing non-aqueous electrolytes, the internal electrolyte resistance is usually appreciably higher than for aqueous solutions but this is compensated by higher operational voltage, which enters ''squared'' into the energy density.

* Corresponding author. Tel.: +1-613-562-5481; fax: +1-613-562-5170.

0378-7753/01/$ – see front matter © 2001 Elsevier Science B.V. All rights reserved.
PII: S0378-7753(00)00682-0

A pure capacitance, such as that of the double-layer [6], can be discharged at high rates, limited only by a (usually small) equivalent series resistance (ESR). However, in the case of electrochemical capacitors based on high-area, porous materials, an unavoidable distributed resistance (R) arises (mainly of the electrolyte in the pores) that is coupled in a complex way with the distributed interfacial capacitance elements (C), giving rise to a distribution of "RC" time-constants and a resultant power spectrum. This situation was treated in mathematical detail by de Levie [12,13] in a series of papers. The important general conclusions, relevant to porous capacitor behaviour, were: (a) that a so-called "penetration effect" (into the porous matrix) applies to any time-dependent electrical signal — current pulse, potential pulse or amplitude voltage (a.v.) modulation — so the charging or discharging response function is time-dependent; and (b) that the overall behaviour under a.v. modulation is a transfer function characterised by a -45° phase angle of the impedance vector, represented in the complex-plane.

These aspects, treated by de Levie [12] and later by Keiser et al. [14] for pores of various shapes, provide the foundations for consideration of power limitations in the operation of electrochemical capacitor devices based on high-area, porous electrode materials.

Because of the relationship between the response currents, I, to repetitive linear voltage modulation (cyclic voltammetry (CV)) at sweep rates $s = \pm \mathrm{d}V/\mathrm{d}t$, giving directly the capacitance $C = I/s$, CV has become a major procedure for evaluating performance of capacitor devices. It is convenient for determining cycle life, and from analysis of the shapes of the response-current voltammograms as a function of s, it provides information on internal resistance effects and consequent dissipative losses.

The present paper examines consequences of such effects in quantitative ways, through simulation calculations, especially for cases where the performance characteristics are evaluated by means of CV and dc charging curves. The results of simulation calculations for various conditions applied to voltammetry and dc charging behaviour at porous capacitor electrodes are compared with experimental results obtained at specially fabricated, non-aqueous electrolyte capacitor modules containing sub-optimal electrolyte concentrations in order to enhance internal resistance effects, thus, enabling them to be more quantitatively characterizable.

2. Treatment of cyclic voltammetry (CV) and dc charging at porous electrodes

Equations have been developed for potentiostatic and galvanostatic charging transients at porous and tubular electrodes of finite length in the absence of appreciable Faradaic currents, for systems of *constant* electrolyte resistance [15,16]. The case of linear or triangular voltage sweep (CV) in the presence of significant, but *constant*, IR drop for porous electrodes was considered in detail by Austin and Gagnon [17].

Effects of internal electrolyte resistance and its changes under certain conditions during charging and discharging of porous capacitor electrodes are examined here for cases of charge/discharge under CV and for dc constant current cycling. The required mathematical equations are developed and their solutions are evaluated with numerical simulations for various conditions.

The assumptions made in the calculations include the following:

1. that the double-layer capacitance, C, is constant over the voltage window of operation;
2. only capacitative processes occur, i.e. there is no Faradaic charging;
3. only ohmic losses are considered;
4. the electrolyte conductivity is either (1) constant, or (2) a linear function of the local potential at the working electrode.

3. Governing equations

The current response, $I(V_\mathrm{m})$ at a potential V_m, for a purely capacitative process, involving a constant capacitance, C, is given by:

$$I(V_\mathrm{m}) = C\left(\frac{\mathrm{d}V_\mathrm{e}}{\mathrm{d}t}\right) \tag{1}$$

where V_m is the measured potential and V_e the local potential at the capacitative electrode. V_e differs from V_m by the "IR" loss due to potential dependent passage of response current when the system includes a significant series resistance.

3.1. Constant electrolyte resistance

The local electrode potential, during the anodic direction of polarisation of a CV experiment, between the applied potential limits of V_1 and V_2, assuming the presence of a constant electrolyte series resistance, R_0, is

$$V_\mathrm{e} = V_1 + st - IR_0 \tag{2a}$$

and during the cathodic direction of the CV, between the applied potential limits of V_2 and V_1, is

$$V_\mathrm{e} = V_2 - st - IR_0 \tag{2b}$$

where s is the applied potential sweep rate, $\mathrm{d}V/\mathrm{d}t$. Differentiating Eqs. (2a) and (2b) with respect to t, and substituting for $\mathrm{d}V/\mathrm{d}t$ in Eq. (1), results in the following first-order differential equation for anodic current $I_\mathrm{a}(V_\mathrm{m})$

$$I_\mathrm{a}(V_\mathrm{m}) = Cs - R_0 C\frac{\mathrm{d}I_\mathrm{a}}{\mathrm{d}t} \quad \text{for} \quad 0 \le t \le \frac{(V_2 - V_1)}{s} \tag{3a}$$

and for cathodic current $I_c(V_e)$

$$I_c(V_m) = -Cs - R_0 C\frac{dI_c}{dt}$$
$$\text{for} \quad \frac{(V_2 - V_1)}{s} \le t \le \frac{2(V_2 - V_1)}{s} \tag{3b}$$

The analytical solutions of Eqs. (3a) and (3b), subject to the boundary conditions

$$I_a(t = 0) = I_c\left(t = \frac{2(V_2 - V_1)}{s}\right) \tag{4a}$$

and

$$I_a\left(t = \frac{(V_2 - V_1)}{s}\right) = I_c\left(t = \frac{(V_2 - V_1)}{s}\right) \tag{4b}$$

are

$$I_a = sC - \left(\frac{2sC}{1 + \exp((V_1 - V_2)/sR_0C)}\right)\exp\left(-\frac{t}{R_0C}\right)$$
$$\text{for} \quad 0 \le t \le \frac{(V_2 - V_1)}{s} \tag{5a}$$

and

$$I_c = -sC + \left(\frac{2sC}{1 + \exp((V_1 - V_2)/sR_0C)}\right) \times \exp\left(\frac{(V_2 - V_1)/s - t}{R_0C}\right)$$
$$\text{for} \quad \frac{(V_2 - V_1)}{s} \le t \le \frac{2(V_2 - V_1)}{s}. \tag{5b}$$

3.2. Case for electrolyte being consumed during charging of the capacitor

Consider, next, the case in which, during the course of charging of the capacitative electrode, the electrolyte is "consumed" and, as an approximation, the electrolyte resistance then becomes a linear function of the local electrode potential, thus

$$R = R_0 + rV_e \tag{6}$$

In real, two-electrode, high-area capacitor device this "consumption" of electrolyte from the bulk solution is a measurable effect and arises because of differential cation/anion adsorption between the two electrodes as the their double-layers become charged [18,19].

As a result of Eq. (6), the local potential, V_e, during the anodic direction of polarisation in a CV experiment, conducted between the applied potential limits of $V_m = V_1$ and $V_m = V_2$, is

$$V_e = V_1 + st - IR_0 - IrV_e$$
$$\text{or} \quad V_e = (V_1 + st - IR_0)(1 + Ir)^{-1} \tag{7a}$$

while during the cathodic direction of a CV experiment, between the applied potential limits of V_2 and V_1, V_e is

$$V_e = (2V_2 - V_1 - st - IR_0)(1 + Ir)^{-1} \tag{7b}$$

After differentiating Eqs. (7a) and (7b) with respect to t and substituting into Eq. (1), the following expressions for current as a function of time result:

$$I_a = \frac{Cs(1 + Ir) - C(R_0 + rV_1 + rst)(dI/dt)}{(1 + Ir)^2}$$
$$\text{for} \quad 0 \le t \le \frac{V_2 - V_1}{s} \tag{8a}$$

and

$$I_a = \frac{-Cs(1 + Ir) - C(R_0 + 2rV_2 - rV_1 - rst)(dI/dt)}{(1 + Ir)^2}$$
$$\text{for} \quad \frac{V_2 - V_1}{s} \le t \le \frac{2(V_2 - V_1)}{s} \tag{8b}$$

A numerical solution, subject to the boundary conditions of Eq. (4a) and (4b), may be determined using the Euler–Cauchy method [20], since the change in current with time may be expressed as

$$\frac{dI_a}{dt} = \frac{CsIr + Cs - I - 2I^2r - I^3r^2}{CR_0 + CrV_1 + Crst}$$
$$\text{for} \quad 0 \le t \le \frac{V_2 - V_1}{s} \tag{9a}$$

and

$$\frac{dI_c}{dt} = \frac{-CsIr - Cs - 2I^2r - I^3r^2}{CR_0 + 2CrV_2 - CrV_1 - Crst}$$
$$\text{for} \quad \frac{V_2 - V_1}{s} \le t \le \frac{2(V_2 - V_1)}{s} \tag{9b}$$

with an initial value of $I_a(t = 0)$ being assumed. The numerical solution determined using Eqs. (9a) and (9b), for given R_0 and $r = 0$ was identical to the analytical solution calculated using Eqs. (5a) and (5b).

3.3. Case for electrolyte being consumed during constant current charging of the capacitor

The electrical response during charge/discharge is governed by Eq. (1), but becomes simplified in the case of constant current to:

$$\Delta V_e = \frac{I}{C}\Delta t \tag{10}$$

Given that the measured voltage includes the *IR* component, it may be calculated simply as

$$V_m = V_e(1 + Ir) + IR_0 \tag{11}$$

i.e. V_m is determined both by the intrinsic resistance, R_0, of the electrolyte medium and its change with polarisation potential expressed by r in Eq. (6).

4. Experimental

4.1. Comparisons with behaviour of real capacitor modules

In order to examine the validity of the simulation treatments developed in Section 3, comparisons were made

experimentally with the charge/discharge behaviour of two specially fabricated, non-aqueous porous carbon electrodes, described below. The experimental test procedures employed CV conducted at various sweep-rates and dc charge/discharge cycling at various currents.

The temperature for all experiments was $25 \pm 1^{\circ}$C. Electrical connections to the modules from the potentiostat were made in a two-electrode configuration, with one of the two capacitor electrodes serving both as a counter and reference (positive terminal).

4.2. Capacitor module fabrication

Type 14–50 (size R6/AA) hardware was used to construct the sealed single-cell electrochemical capacitor modules used in these tests. The porous electrode modules employed 1.0 and 0.40 M tetraethylammonium tetrafluoroborate (TEATFB) in dry propylene carbonate as electrolyte, as described elsewhere [18].

5. ResuIts and their interpretations

5.1. Calculated CV responses

5.1.1. Case of constant resistance (R_0)

In Fig. 1, current responses are conveniently plotted as reduced currents ($I(V_m)/sC$) as a function of measured potential ($V_e + IR_0$), of a capacitative electrode exposed to electrolytes having various constant electrolyte resistances, R_0, between 0 and 50 Ω, ($C = 1$ F, $s = 20$ mV s^{-1}, $V_1 = 0$ V, $V_2 = 1$ V) as previously discussed in some detail [21]. For sufficiently small resistance, R_0, the current response is essentially that of a pure capacitor (Fig. 1 for $R_0 \rightarrow 1$ Ω). Increasing R_0 increases the IR_0 component and, given a sufficiently large R_0, the overall behaviour of the resistor/capacitor network becomes dominated by the resistive component. Note also, that the form of the CV calculated for the constant resistivity simulation is symmetrical with respect to an in-plane rotation of 180° which renders the I_a/sC^{-1} versus V response superimposable with the reverse scan. This indicates that the beginning of discharge behaves identically to the beginning of charge with the exception of reversal in the direction of current.

Examination of the reduced current as a function of the local electrode potential, V_e, (Fig. 1b) illustrates, given a sufficiently large resistance and resulting IR_0 loss component, how the applied and actual potentials are significantly different so that the actual sweep rate at the working electrode and the effective range of applied potential is far from what the experimenter intended. As well, the local sweep rate, dV_e/dt, for large R_0, is not constant, and the I/sC^{-1} versus V_e response is not of the expected rectangular form for a purely capacitative device.

Correspondingly, similar behaviour results with increasing capacitance, C, and/or sweep rate, s, while maintaining a given fixed resistance value. In the former case, an increase in device capacitance, C, results in an increase in the current I passed (Eq. (1)), and hence an increase in the IR_0 losses. In the latter case, at low sweep rate, I is small, so that IR_0 losses are negligible, but as the applied sweep rate is increased, the current increases, so that IR_0 losses become significant. The dependence of "effective" capacitance on sweep rate is of particular importance as it provides an indication of the rate performance of the electrode, i.e. a high sweep rate corresponds to a high rate of charge or discharge of the capacitor electrode, corresponding to greater power levels of operation.

Importantly, these results show that even though the actual capacitance of the working electrode is constant and independent of either R_0 or s, the "effective" capacitance, which is determined by the IR_0 component, is not constant. Rather, the effective capacitance decreases with increasing R_0 and/or s, and is typically much less than C. Thus, less and less of the "theoretical" charge capacity is accessible with increasing R_0 and/or s, leading to diminution of energy–density and power–density of the device modelled by the above equations.

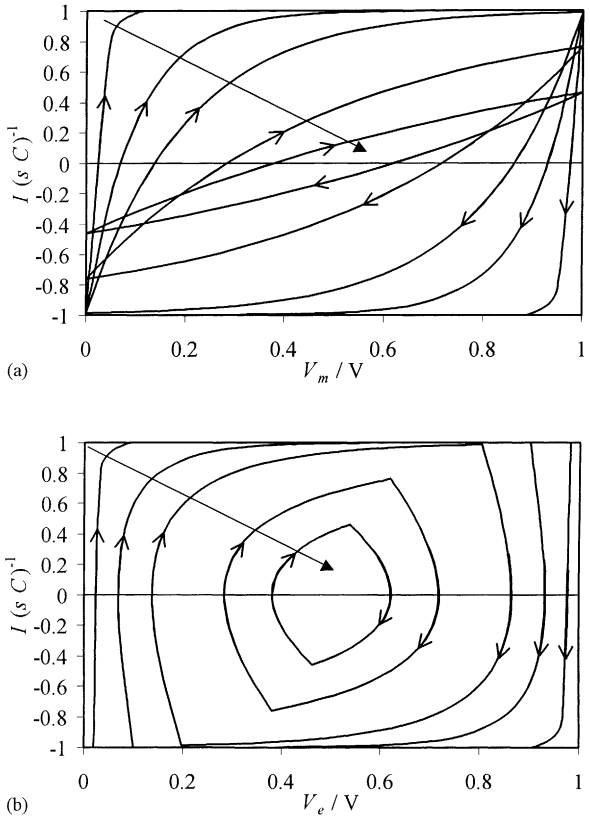

Fig. 1. Calculated cyclic voltammograms expressed as reduced response current (I/sC) as a function of (a) measured potential ($V_e + IR_0$) and (b) local working electrode potential (V_e) calculated using Eqs. (5a) and (5b) for $C = 1$ F, $V_1 = 0$ V, $V_2 = 1$ V, $s = 20$ mV s^{-1}. (⇑) Indicates direction of increasing R_0 (1, 5, 10. 25 and 50 Ω); (⟶) direction of voltammetric sweep.

5.1.2. Case where R a linear function of the local working electrode potential

We now examine, in some detail, the results of simulation calculations for a capacitative electrode subject to increasing electrolyte resistivity with increasing state-of-charge, i.e. subject to a resistance component dependent on V_e as represented by Eq. (6). The effects of the variable resistance on the CV response for three distinct cases are examined: (a) constant s, C and r (the voltage-dependent component of resistance), and various values of the so-called "fixed" component of the resistance, R_0 (b) constant s, C and R_0, and various values of the voltage-dependent component of resistance, r; and (c) various sweep rates for selected C, R_0 and r values.

Two cases each for $s = 20\ \text{mV s}^{-1}$, $C = 1\ \text{F}$ and $R_0 = 1$, 5, 10, 25 and 50Ω are considered: the first taking $r = 1\ \Omega\ \text{V}^{-1}$ in Eq. (6) and the second $r = 5\ \Omega\ \text{V}^{-1}$. Plots of reduced current as a function of measured potential for $r = 1\ \Omega\ \text{V}^{-1}$, together with that for $r = 0\ \Omega\ \text{V}^{-1}$, for various R_0 values are shown in Fig. 2a. The complementary plot of reduced current as a function of local electrode potential is shown in Fig. 2b.

Upon examination of Fig. 2a, it is clear that, for a small r to R_0 ratio ($r/R_0 < 1\ \text{V}^{-1}$), the anodic scan remains essentially unchanged from that for the $r = 0\ \Omega\ \text{V}^{-1}$ case, whereas the cathodic reduced current response is initially more sloping (i.e. resistive). Toward the less positive potential limit of the cathodic scan, the reduced current response is again superimposable upon the response for $r = 0\ \Omega\ \text{V}^{-1}$. Note that the reduced current response for $r = 1\ \Omega\ \text{V}^{-1}$ does not exhibit the same symmetry as for the $r = 0\ \Omega\ \text{V}^{-1}$ case. From Fig. 2b, it is clear that the r component further limits the upper voltage window of operation, and thus reduces the power the electrode is capable of delivering.

If r is comparable to or larger than R_0 (Fig. 3a and b), then both the anodic and cathodic reduced current responses are modified. In this case, the anodic side of the CV has the same general shape as for the case when $r = 0\ \Omega\ \text{V}^{-1}$, but the maximum reduced current, I/sC^{-1}, achieved is <1. Again, the cathodic response at more positive potentials, is more sloping and interestingly, the reduced current at less positive potentials can be greater than I (Fig. 3 for $r = 5\ \Omega\ \text{V}^{-1}$ and $R_0 = 1,\ 5,\ 10\ \Omega$). For these cases, the plots of reduced current as a function of local or measured potentials are

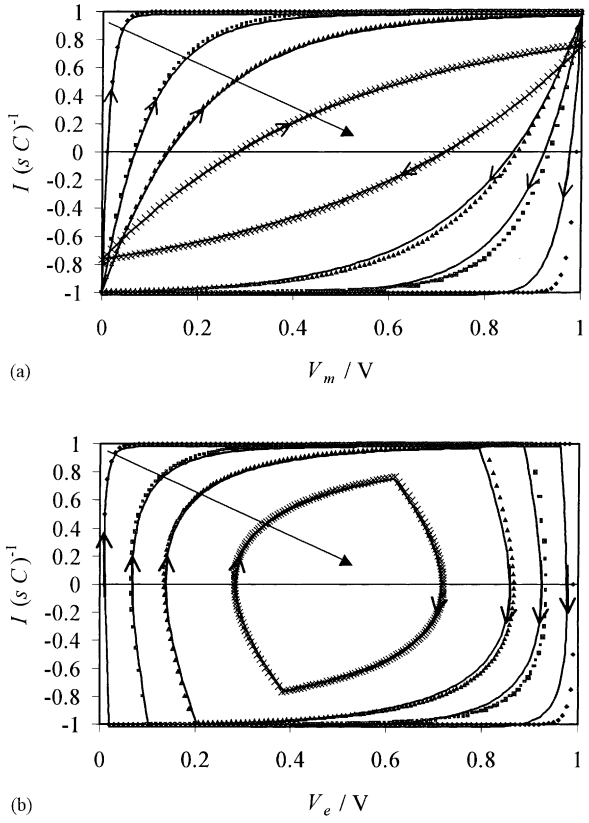

Fig. 2. Calculated cyclic voltammograms expressed as reduced response current (I/sC) as a function of (a) measured potential ($V_e + I(R_0 + rV_e)$) and (b) local working electrode potential (V_e) calculated using Eqs. (8) and (9) for $C = 1\ \text{F}$, $V_1 = 0\ \text{V}$, $V_2 = 1\ \text{V}$, $s = 20\ \text{mV s}^{-1}$. Solid curves $r = 1\ \Omega\ \text{V}^{-1}$ and symbols $r = 0\ \Omega\ \text{V}^{-1}$; (⇑) Indicates direction of increasing R_0 (1, 5, 10 and 25 Ω); (⟶) direction of voltammetric sweep.

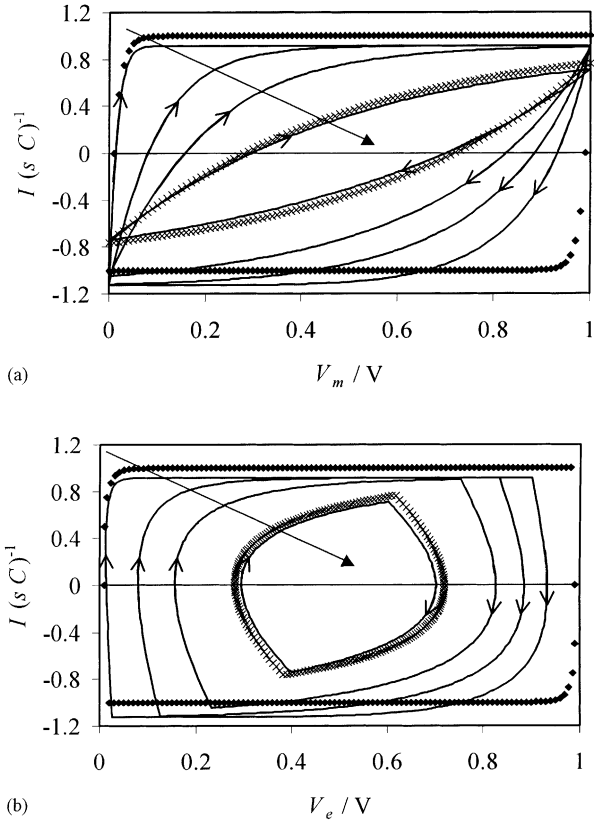

Fig. 3. Calculated cyclic voltammograms expressed as reduced response current (I/sC) as a function of (a) measured potential ($V_e + I(R_0 + rV_e)$) and (b) local working electrode potential (V_e) calculated using Eqs. (8) and (9) for $C = 1\ \text{F}$, $V_1 = 0\ \text{V}$, $V_2 = 1\ \text{V}$, $s = 20\ \text{mV s}^{-1}$. Solid curves $r = 5\ \Omega\ \text{V}^{-1}$ and symbols $r = 0\ \Omega\ \text{V}^{-1}$; (⇑) indicates direction of increasing R_0 (1, 5, 10 and 25 Ω); (⟶) direction of voltammetric sweep.

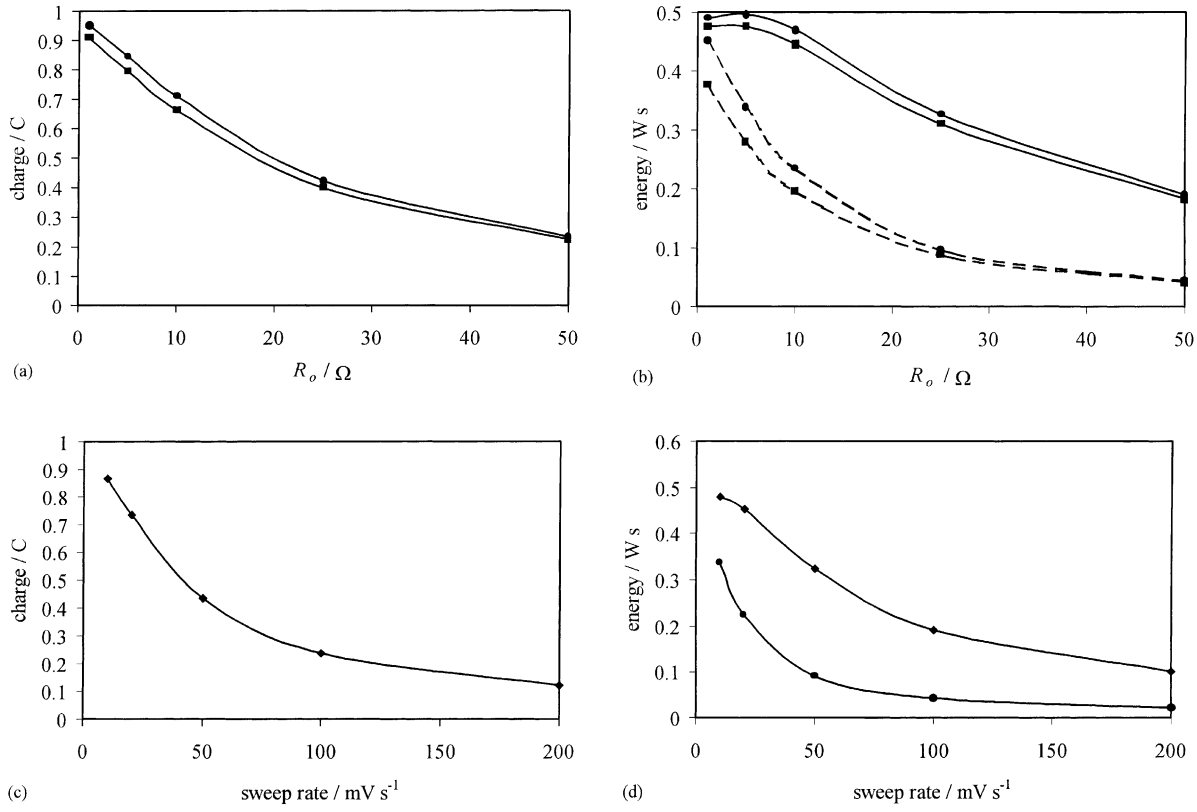

Fig. 4. (a) Charge and (b) energy as a function of R_0, calculated from the CV's shown in Figs. 2 and 3: (●) $r = 1$; (■) $r = 5$; (—) charge cycle; (- - -) discharge cycle.

highly asymmetric, indicating that the local electrode sweep rate, dV_e/dt, can, under certain conditions, be larger than s.

In Fig. 4a, the charge capacity, Q in (As) calculated from the CV's shown in Figs. 2 and 3. The charge efficiency determined as $(Q_{output}/Q_{input}) \times 100$ was calculated to be constant and approximately 100% for all values of R_0 and r. The energy realisable on discharge of the capacitor electrode, especially for cases of large R_0, will, however, be much less than that involved in charging the same electrode, thus corresponding to serious dissipative losses. This is clearly shown in Fig. 4b in which the energies required for charge and delivered on discharge are plotted as a tunction of R_0. The energy efficiency, of course, decreases with increasing R_0. For $r/R_0 < 0.5\ V^{-1}$, the absolute maximum reduced anodic or cathodic current densities are <1, and the CVs become more symmetrical.

In Fig. 5a and b, the effect of increasing the ratio of r/R_0 on the reduced current as a function of reduced and local electrode potentials, respectively, is examined for a given constant sweep rate of 20 mV s^{-1}, a constant capacitance of 1 F, a fixed and significant value of $R_0 = 10\ \Omega$ and r/R_0 values of 0, 0.1, 1, 2, 5 and 7.5 V^{-1}. In Fig. 5c, the calculated charge capacity (i.e. charge, Q) and the energy required for charge and that delivered on discharge for the CV's shown in Fig. 5a and b.

Again, the CV response is not symmetric about the $I/sC = 0$ line, and the degree of asymmetry increases with increasing r value. As r is increased, the anodic scan becomes more sloping and the maximum anodic current achieved decreases as does the total charge. The cathodic scan response is more complicated. Increasing r, initially causes the cathodic response to be more sloping, and the maximum reduced current to be >1, further increase of r results in an even more sloping CV response, and reduced currents <1. A plot of the reduced current versus local potential (Fig. 5b) at the working electrode illustrates that increasing r reduces the potential range over which the working electrode actually cycles.

The effect of reducing the potential range over which the working electrode cycles is shown quantitatively in Fig. 5c in which electrode charge capacity is plotted as a function of r. In fact, Q is a linear function of the magnitude of the potential range over which the working electrode actually cycles, ΔV_e, as shown in the inset of Fig. 5c. Although the charge capacity decreases with r, the charge efficiency is independent of r and approximately 100%. Both the energy required for charge and that delivered on discharge decrease with increase in r (Fig. 5d), as does the energy efficiency.

Finally, the effect of sweep rate on CV response for a system defined by $C = 1$ F, $R_0 = 5\ \Omega$, $r = 10\ \Omega\ V^{-1}$ and $s = 10$, 20, 50, 100 and 200 mV s^{-1} is shown in Fig. 6. At

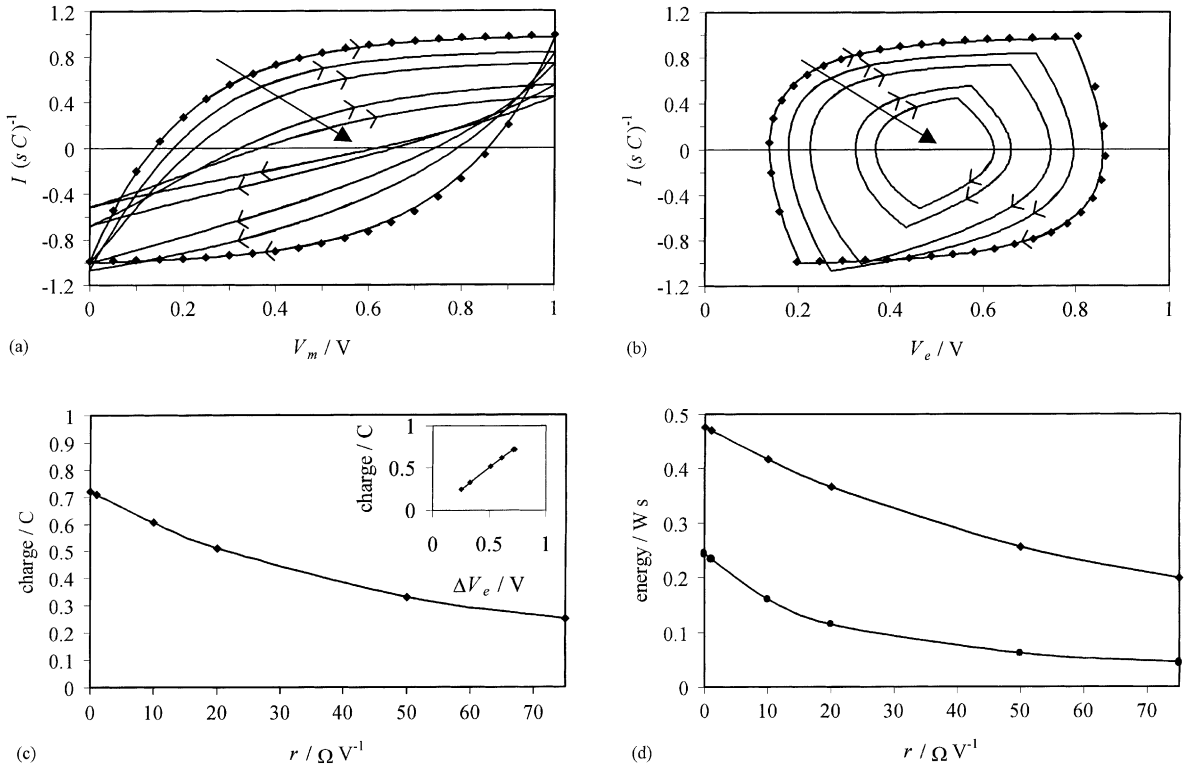

Fig. 5. Calculated cyclic voltammograms expressed as reduced response current (I/sC) as a function of (a) measured potential ($V_e + I(R_0 + rV_e)$) and (b) local working electrode potential (V_e) calculated using Eqs. (8) and (9) for $C = 1$ F, $V_1 = 0$ V, $V_2 = 1$ V, $s = 20$ mV s^{-1}, $R_0 = 10\ \Omega$, symbols $r = 0\ \Omega\ V^{-1}$. Solid curves $r = 1$, 10, 20, 50 and 75 $\Omega\ V^{-1}$; (⇑) indicates direction of increasing r; (→) direction of voltammetric sweep. (c) Charge and (d) energy as a function of r calculated from the CV's shown in (a) and (b): (◆) charge cycle; (●) discharge cycle. (c) Charge as a function of ΔV_e from CV's shown in (a) and (b).

low sweep rate (10, 20 and 50 mV s^{-1}), the cathodic current response deviates from the ideal rectangular response much more than does the anodic response. Consider first the anodic scan at low sweep rate; at low potential, the local electrode potential is approximately the same as the measured potential, and the electrolyte resistance is simply R_0. At higher potential, however, the rV_e component of the resistance becomes significant resulting in a limiting value for reduced current <1. This IrV_e component then results in a sloping cathodic current response which causes the cathodic response over the full potential range to be far from ideal.

As sweep rate increases, *IR* on both anodic and cathodic sweeps increases and both anodic and cathodic responses deviate from the rectangular ideal form, ($s = 100$ and 200 mV s^{-1}). Further, the voltage range over which the working electrode operates becomes greatly reduced (Fig. 6b), as does the charge capacity of the electrode which falls from 1 C at $s = 0$ mV s^{-1}, to 0.12 C at $s = 200$ mV s^{-1}. Again, the charge efficiency independent of s and 100%.

In Fig. 6d, the plot is of energy to charge and the energy recovered on discharge as a function of s. Both quantities are found to decrease with increase in s (i.e. decrease with increase in charge/discharge rate), as is the energy efficiency because increase in five results in an increase in both the IR_0 and IrV_e losses.

5.2. Calculated constant current charge/discharge behaviour

Three cases are considered for a capacitative electrode having a capacitance of 1 F operating within a voltage window of 1 V: (a) constant I, r and various R_0; (b) constant I, R_0 and various r; and (c) constant r, R_0 and various constant currents.

5.2.1. Case (a)

As R_0 increases the "*IR*" step which arises at the beginning of charge and discharge increases as seen in the V_m versus t plots of Fig. 7a for second and subsequent charge/discharge cycles of an electrode having $C = 1$ F, ΔV(measured) = 1 V, $I = 10$ mA, $r = 5\ \Omega\ V^{-1}$ and $R_0 = 0$, 1, 5, 10 and 25 Ω. As a result, the total time of charging to a given voltage limit ($V_m = V_2$) decreases with increased R_0 (therefore, the electrode has less effective charge capacity within a particular voltage window). Also, the average voltage on charge is greater than the average on discharge; as a result, power consumption during charging will be greater than power available on discharge (i.e. watt-hour efficiency will be low, and decrease with increasing R_0), a significant practical conclusion. In Fig. 7b, the local electrode potential, V_e, as a function of time during charge/discharge between measured potential limits of 0 and 1 V.

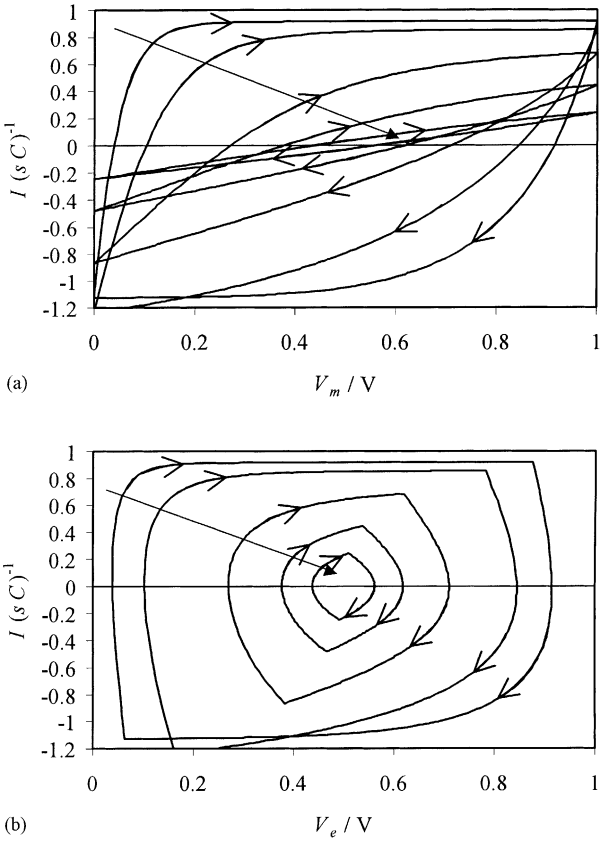

Fig. 6. Calculated cyclic voltammograms expressed as reduced response current (I/sC) as a function of (a measured potential ($V_e + I(R_0 + rV_e)$) and (b) local working electrode potential (V_e) calculated using Eqs. (8) and (9) for $C = 1$ F, $V_1 = 0$ V, $V_2 = 1$ V, $R_0 = 10\,\Omega$, $r = 10\,\Omega\,V^{-1}$. (⇑) Indicates direction of increasing s; (→) direction of voltamrnetric sweep. (c) Charge and (d) energy calculated from the CV's shown in (a) and (b): (◆) charge cycle; (●) discharge cycle.

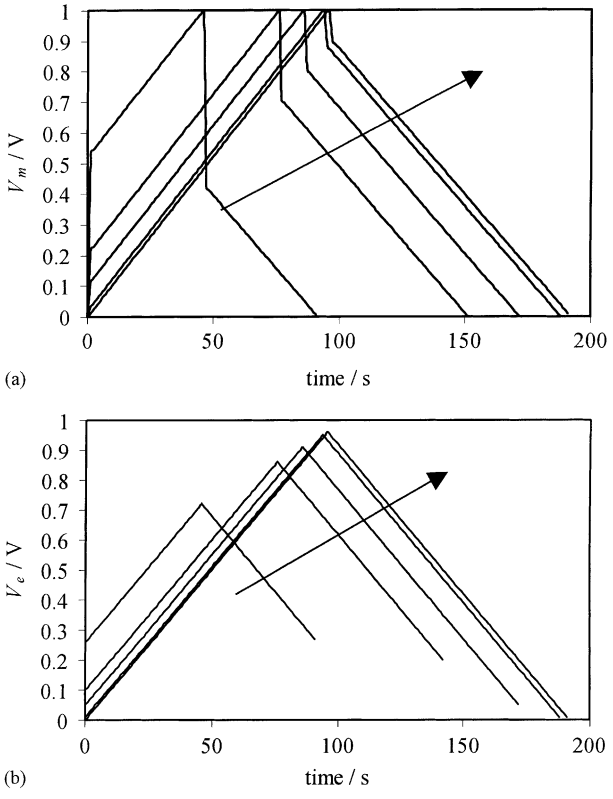

Fig. 7. Calculated voltage profile for second constant current charge/discharge cycle as a function of time using Eq. (11) for $C = 1$ F, $V_1 = 0$ V, $V_2 = 1$ V, $I = 10$ mA, $r = 5\,\Omega\,V^{-1}$: (a) measured potential ($V_e + I(R_0 + rV_e)$) and (b) local working electrode potential (V_e). (⇑) Indicates direction of decreasing R_0 (25, 10, 5, 1 and 0 Ω).

Clearly, the capacitative electrode is cycling within a restricted potential range, which decreases with increasing R_0. Note also that increasing R_0 both decreases the anodic potential limit and increases the cathodic limit, thus reducing the cycling window at both extremes of potential.

5.2.2. Case (b)

Fig. 8a and b plotted the V_m and V_e versus t, respectively, for an electrode defined by $C = 1$ F, ΔV(measured) $= 1$ V, $I = 10$ mA, $R_0 = 10$ and r of 0, 10, 20, 35, 50 and 75 $\Omega\,V^{-1}$. The IR drop on switching from discharge to recharge is determined primarily by R_0 (except in the case of very large r/R_0), while that for switching from charge to discharge is due to the combination of r and R_0 terms. Interestingly, however, the working electrode reversal potential on the second and subsequent charge is determined by the magnitude of r. Again, increasing r will lower both watt-hour efficiency (due to higher charging voltage as compared with discharge voltage) and charge storage capacity (as r increases the local working electrode cycling range decreases).

5.2.3. Case (c)

The rate effects for a system having $C = 1$ F, ΔV (measured) $= 1$ V, $R_0 = 5\,\Omega$ and $r = 10\,\Omega\,V^{-1}$ and $I = 10$, 20, 30 and 40 mA are shown in Fig. 9a and b for measured and local electrode potentials, respectively, as a function of charge (mAh) for second and subsequent charge/discharges. The effective electrode charge capacity (Ah) and effective capacitance (F) are both rate dependent. Capacity (Ah) decreases with increasing I (and consequently increasing IR). As the current increases the effective capacitance increases, but over a progressively decreasing voltage window. The charging efficiency (Ah) remains relatively constant with increasing I (≥90%). Similar to the results shown in Figs. 7 and 8, increasing rate results in a restriction of the local potential cycling range. Similar trends are shown in the three Figs. 7–9 where it is seen that each of increasing R_0, r and I results in an increase in the "IR" loss component.

5.3. Comparison with experimental results for specially prepared non-aqueous carbon electrode supercapacitors

5.3.1. Cyclic voltammetry (CV)

The experimentally derived capacitance response voltammograms for specially prepared [18] capacitor devices

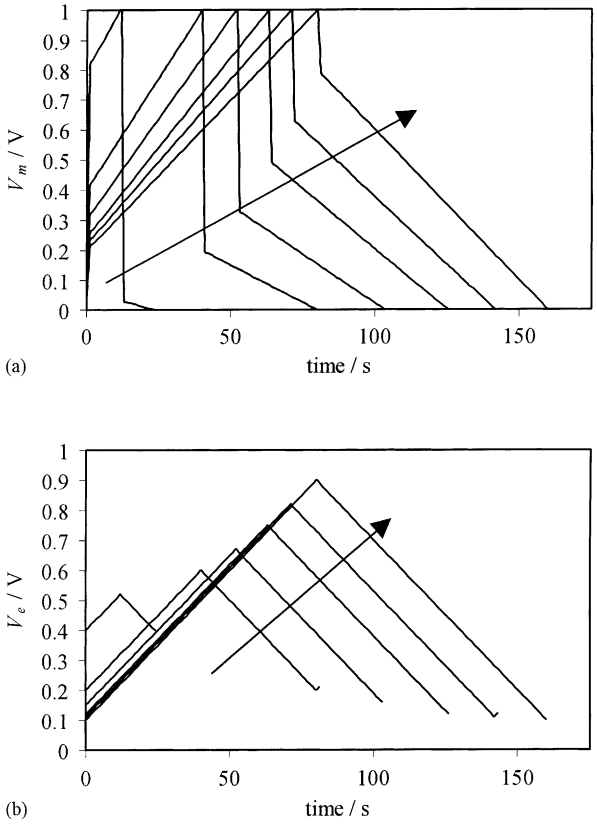

Fig. 8. Calculated voltage profile for second constant current charge/discharge cycle as a function of time using Eq. (11) for $C = 1$ F, $V_1 = 0$ V, $V_2 = 1$ V, $I = 10$ mA, $R_0 = 10\ \Omega$: (a) measured potential ($V_e + I(R_0 + rV_e)$) and (b) local working electrode potential (V_e). (⇑) Indicates direction of decreasing $r = 0$, 10, 20, 35, 50 and 75 $\Omega\ V^{-1}$.

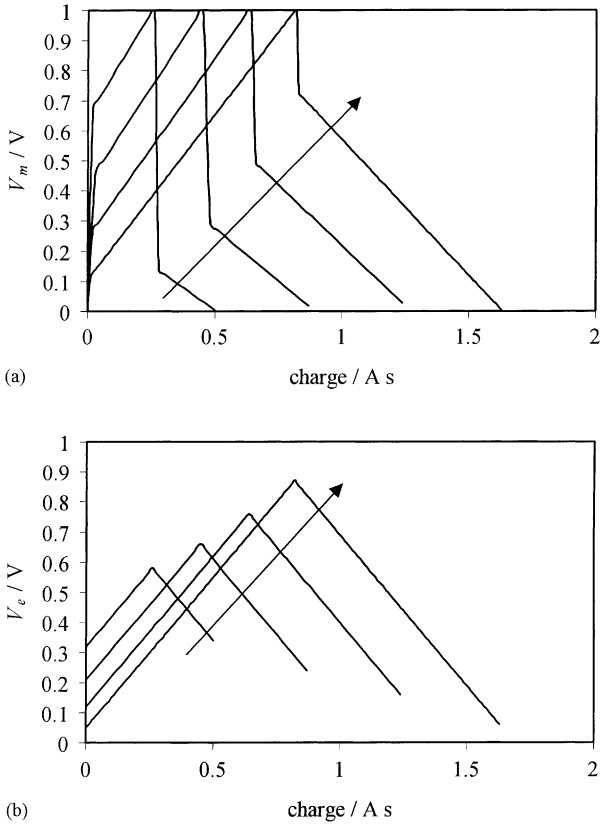

Fig. 9. Calculated voltage profile for second constant current charge/discharge cycle as a function of time using Eq. (11) for $C = 1$ F, $V_1 = 0$ V, $V_2 = 1$ V, $R_0 = 5\ \Omega$, $r = 10\ \Omega\ V^{-1}$: (a) measured potential ($V_e + 1(R_0 + rV_e)$) and (b) local working electrode potential (V_e). (⇑) Indicates direction of decreasing $I = 10$, 20, 30 and 40 mA.

having 1.0 and 0.4 M TEATFB electrolyte are shown in Fig. 10a and b, respectively, as a function of sweep-rate.

In Fig. 10a, for the 1.0 M electrolyte, the capacitance behaviour approximates to ideal behaviour at the lowest sweep-rate of 1 mV s^{-1}, i.e. a voltammogram having an almost rectangular form and mirror-image symmetry of the current responses about the zero-current line is observed. With increasing s the voltammograms become distorted from the rectangular form expected for an ideal capacitor having constant capacitance, similar to the calculated effects shown in Fig. 1.

The CV response of the module made with 0.4 M electrolyte, shown in Fig. 10b, for $s = 5$, 10, 20, 30 and 40 mV s^{-1}, exhibits behaviour similar to that calculated for the significant resistance models of this study (cf. Fig. 2). Here the capacitance response as a function of voltage is nearly ideal at low sweep rate (5 mV s^{-1}), while at higher sweep rates, becomes distorted. At high s, unlike the ideal behaviour, the realised capacitance is both varying with module voltage and increasing with decreasing s.

5.3.2. Constant-current charge/discharge behaviour

The observed constant-current charge/discharge behaviour is plotted in Fig. 11a and b for the respective capacitor modules discussed in Section 5.3.1, having 1.0 and 0.4 M electrolyte, respectively, as a function of calculated cumulative charge, Q, in As at constant current charge/discharge rates of 1.33, 1.0, 0.67, 0.33 A g^{-1} of carbon.

Note, even for the 1.0 M module shown in Fig. 11a, that there is a small, but significant sharp drop in voltage on changing from charging to discharging current and a sharp increase at the start of the charging process. This is not due entirely to a direct ESR effect but is also a characteristic of *redistribution* of charge within the pores. The same characteristic curve was demonstrated in [22] found for a hardware, four-element model RC network, made with relatively small resistive elements. Probe measurements enabled redistribution of charge at each of the capacitor elements in this hardware RC ladder network to be directly observed experimentally [22].

Fig. 11b shows similar plots for the capacitors employing the smaller concentration of electrolyte, 0.4 M. Here the *IR* drops are significantly larger than those in Fig. 11a, and even at the lowest rate of charge/discharge of 0.25 A, the charge capacity of the 0.4 M electrolyte module is significantly reduced from that of the 1.0 M module. This further illustrates that in the low concentration electrolyte modules the local electrode potential range is much smaller than the

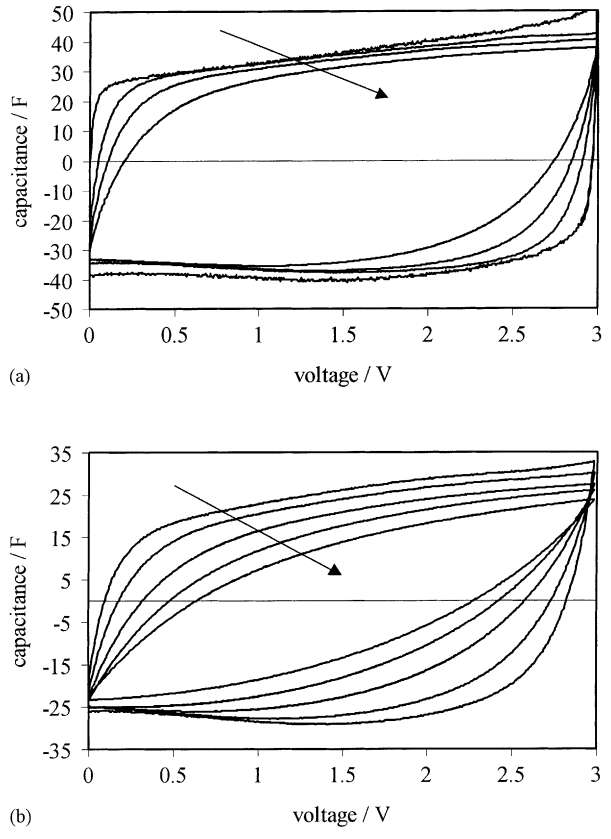

Fig. 10. (a) Cyclic voltammograms, showing the current responses expressed as capacitance, for the 1.0 M TEATFB electrolyte module as a function of voltage over the voltage range 0–3 V at 1, 5, 10 and 20 mV s^{-1}; arrow indicates direction of increasing sweep rate; (b) cyclic voltammograms, showing the current responses expressed as capacitance, for the 0.4 M TEATFB electrolyte module as a function of voltage over the voltage range 0–3 V at 5, 10, 20, 30 and 40 mV s^{-1}. (⇑) Indicates direction of increasing sweep rate.

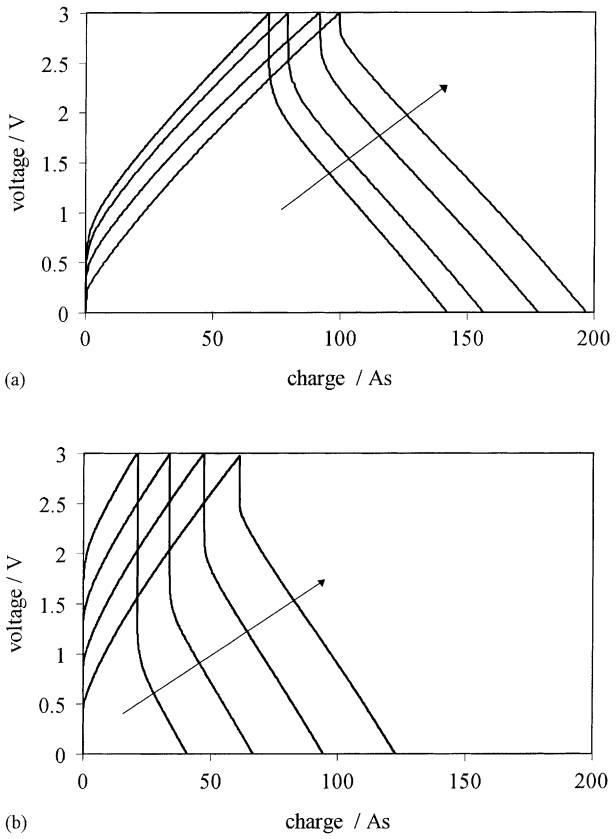

Fig. 11. The voltage response to constant current charging/discharging currents of 1.33, 1.0, 0.67 and 0.33 A g^{-1} of carbon, as a function of cumulative calculated charge (As) for a redox engineering 3 V AA electrochemical capacitor: (a) electrolyte concentration 1.0 M, and (b) electrolyte concentration 0.4 M. (⇑) Indicates the direction of decreasing current density.

measured range. Thus, *IR* effects can result in reduced energy– and power–density, and therefore, performance characteristics of practical devices. A rate increase of 0.33–1.33 A g^{-1} of carbon results in a reduction of the charge capacity from 0.99 to 0.72 As (30% reduction) for the 1.0 M electrolyte device, and from 0.61 to 0.21 As (66% reduction) for the 0.4 M electrolyte device. This results from a restriction in the local electrode potential range as previously discussed, and leads to the practically significant reduction in energy storage capacity and energy–density.

These features remain largely unrevealed in constant-current charge/discharge curves for well engineered, practical capacitors having an optimised low resistance of electrolyte, especially in the cases of aqueous electrolyte embodiments.

6. Conclusions

Increasing *s*, *r*, or R_0 results in a decrease in the overall charge storage capacity of the electrode. The ampere-hour efficiency remains, however, constant, at 100% for all *s*, *r* and R_0 considered (i.e. ampere-hour input = ampere-hour output). The energy efficiency (watt-hour output/watt-hour input) was found to decrease with increasing *s*, *r* or R_0. Any variation in *s*, *r* or R_0 which increases the asymmetry of the CV response, results in a decrease in the available energy, and thus a decrease in energy–density an operational energy efficiency. The modelling treatment provides a good computational basis for interpreting the experimental behaviour of selected capacitor test modules.

Acknowledgements

Grateful acknowledgement is made to the Natural Sciences and Engineering Research Council of Canada for support of this work on a Strategic Grant. Thanks are due to Dr. N. Marincic of Redox Engineering Inc. (Winchester, MA) for preparing the non-aqueous solution capacitor modules.

References

[1] B.E. Conway, J. Electrochem. Soc. 138 (1991) 1539.
[2] T.C. Liu, W.G. Pell, B.E. Conway, Electrochim. Acta 42 (1997) 3541.
[3] T.C. Liu, W.G. Pell, B.E. Conway, S. Roberson, J. Electrochem. Soc. 145 (1998) 1882.
[4] Y. Sato, K. Yomogida, T. Nanaumi, K. Kobayakawa, Y. Ohsawa, M. Kawai, Electrochem. Solid State Lett. 3 (2000) 113.
[5] C. Lin, J.A. Ritter, B.N. Popov, J. Electrochem. Soc. 146 (1999) 3155.
[6] D.C. Grahame, Chem. Rev. 41 (1947) 441.
[7] B.E. Conway, Electrochemical Supercapacitors Scientific Fundamentals and Technological Applications, Kluwer-Plenum Publication Company, New York, 1999 (Chapter 10).
[8] B.E. Conway, in: A. Attwell, T. Kelly (Eds.), Power Sources 15 (1995) 65.
[9] J. Miller, in: S. Wolsky, N. Marincic (Eds.), Proceedings of the 4th International Symposium on Double-Layer Capacitors and Similar Energy Storage Devices, Florida Educational Seminars, Boca Raton, FL, 1994.
[10] D. Ragone, in: Proceedings of the Society Automotive Engineers Conference, Detroit, MI, USA, May 1968.
[11] W.G. Pell, B.E. Conway, J. Power Sources 63 (1996) 255.
[12] R. de Levie, Electrochem. Acta 8 (1963) 751.
[13] R. de Levie, Electrochem. Acta 9 (1964) 1231.
[14] H. Keiser, K.D. Beccu, M.A. Gutjahr, Electrochim. Acta 21 (1976) 539.
[15] A.M. Johnson, J. Newman, J. Electrochem. Soc. 118 (1971) 510.
[16] F.A. Posey, T. Morozumi, J. Electrochem. Soc. 113 (1966) 176.
[17] L.G. Austin, E.G. Gagnon, J. Electrochem. Soc. 120 (1973) 251.
[18] W.G. Pell, B.E. Conway, N. Marincic, J. Electroanal. Chem. (2000), in press.
[19] J.P. Zheng, T.R. Jow, J. Electrochem. Soc. 144 (1997) 2417.
[20] F. Kreysig, Advanced Engineering Mathematics, 5th Edition, Wiley, New York, 1983 (Chapter 21).
[21] W.G. Pell, B.E. Conway, J. Electroanal. Chem. (2000), in press.
[22] W.G. Pell, B.E. Conway, W.A. Adams, J. de Oliveira, in: Proceedings of the 21st International Power Sources, Vol. 80, Brighton, UK, 1999, p. 134.